Journal of
Composites Science

MDPI

Article

Powder Metallurgy Preparation and Characterization of Titanium-Titanium Diboride Composite Targeted for Dental Implant

Ali Mohammad Ali Aljafery [1,2], Abdalbseet A. Fatalla [2,*] and Julfikar Haider [3,*]

[1] Department of Prosthodontic, College of Dentistry, University of Kufa, Najaf 54001, Iraq; alim.aljaafri@uokufa.edu.iq
[2] Department of Prosthodontic, College of Dentistry, University of Baghdad, Baghdad 1417, Iraq
[3] Department of Engineering, Manchester Metropolitan University, Manchester M12 5GN, UK
* Correspondence: abdalbasit@codental.uobaghdad.edu.iq (A.A.F.); j.haider@mmu.ac.uk (J.H.)

Abstract: Due to the advantages over other metallic materials, such as superior corrosion resistance, excellent biocompatibility, and favorable mechanical properties, titanium, its alloys and related composites, are frequently utilized in biomedical applications, particularly in orthopedics and dentistry. This work focuses on developing novel titanium-titanium diboride (TiB_2; ceramic material) composites for dental implants where TiB_2 additions were estimated to be 9 wt.%. In a steel mold, Ti-TiB_2 composites were fabricated using a powder metallurgy technique and sintered for five hours at 1200 °C. Microstructural and chemical properties were analyzed by energy dispersive X-ray spectroscopy (EDX), scanning electron microscopy (SEM), and X-ray diffraction (XRD) to evaluate the impact of the TiB_2 ceramic addition. Compressive strength, Brinell hardness, porosity, and density, among other mechanical and physical properties, were also measured and characterized. It has been found that adding TiB_2 to Ti increases its porosity (35.53%), compressive strength (203.04 MPa), and surface hardness (296.3 kg/mm^2) but decreases its density (3.79 gm/cm^3). The lightweight and strong composite could be suitable for dental implant applications.

Keywords: titanium; titanium diboride; powder metallurgy; compressive strength; hardness; density; porosity

Citation: Aljafery, A.M.A.; Fatalla, A.A.; Haider, J. Powder Metallurgy Preparation and Characterization of Titanium-Titanium Diboride Composite Targeted for Dental Implant. *J. Compos. Sci.* **2023**, *7*, 353. https://doi.org/10.3390/jcs7090353

Academic Editor: Francesco Tornabene

Received: 14 July 2023
Revised: 18 August 2023
Accepted: 22 August 2023
Published: 25 August 2023

1. Introduction

Due to the growing life expectancy of the global population, artificial materials implanted surgically to replace natural ones that are missed have emerged as one of the most promising disciplines for enhancing people's quality of life. Due to its exceptional physical, mechanical, and biocompatible qualities, titanium (Ti) is the most frequently used metal in the field of biomaterials. The majority of biocompatible surgical implants available for sale today are made from metals [1,2]. Based on their manufacturing process, titanium alloys can be classified as either powder manufacturing (PM) or cast [3].

Dental implants are one of the most crucial procedures used to replace a missing tooth or teeth because they offer a substitute that is both aesthetically pleasing and functionally satisfying. Dental implants are appliances that replace the natural tooth's missing root in both the mandible and maxilla. Dental implants can act as an anchor for dental prosthetics when they are correctly fabricated and implanted because they eventually bind with bone. According to Brandmark's thorough research, titanium is now the industry standard for dental implants. Yet, a novel, difficult path in implantology has been made possible by the enormous revolution in the sectors of ceramic (e.g., zirconium dioxide) and polymer (e.g., PEEK), as well as other composite materials [4–8].

Although titanium implants have been used successfully, research has continued to focus on the development of sophisticated titanium alloying or reinforcement to improve

the biocompatibility and mechanical qualities. However, thin bones, like the anterior alveolar ridge, are typically ineligible for titanium implant placement [9]. Moreover, bone loss may result from the implant's close contact to nearby teeth [10]. However, due to poor stiffness and wear resistance, their uses are frequently restricted [11]. Titanium based composite, combining the benefits of metal matrix and lightweight ceramic reinforcements, was developed to address these limitations [12]. From the perspective of strengthening theory, the composition, microstructure, and interfacial structure of the composites are directly related to the type of reinforcement included. Controlling the interface between the matrix and the reinforcements is crucial for ensuring the promised strength and stiffness gains in the composites. It has been demonstrated that in situ synthesized reinforcements provide superior characteristics due to the strong connection between the particle and the matrix. Numerous investigations have been conducted on the fabrication, microstructure analysis, and strength improvement of titanium-based composites using various additives, including SiC, Al_2O_3, B_4C, TiN, TiC, and TiB_2. TiB_2 is one of the most compatible precursors for titanium, and is receiving a lot of attention from researchers, because of its high strength, similar density, excellent thermodynamic stability, and similar thermal expansion coefficient to the titanium matrix [13].

Due to its mechanical and thermal stability, as well as the fact that it creates the fewest residual stresses in composites, TiB_2 has recently been found to be the best reinforcement for titanium [14]. Consequently, one of the most wanted titanium matrix composites (TMC) materials is Ti/TiB composites [15]. Numerous studies have been conducted on TiB, not only for grain growth but also to impact α phase's nucleation by presenting a wider variety of potential nucleation sites [16,17]. The phase that crystallizes from TiB also follows the axis of symmetry (001) TiB/(0001) α-Ti, [010] TiB/[11$\bar{2}$0] α-Ti [17]. TiB tends to grow in the [010] direction and has a B27 crystal structure. Since TiB has a hexagonal cross-section and a whisker-like morphology as a result, it may efficiently carry heavier weights due to chemical processes, which can ease the interface limits on the distribution of reinforcements [18]. Also, it was determined that the thermal expansion coefficient and densities of TiB_2 and Ti are almost identical. During the sintering process, TiB_2 reacts with titanium to produce in situ TiB ($Ti + TiB_2 = 2TiB$) [12,19].

Titanium-titanium boride composites can be made using powder metallurgy as one of the primary techniques [20]. The advantages of this technology are microstructural control, fewer material waste, and processing in net shape [21]. In Selvakumar et al. [22], Spark plasma sintering (SPS) vs. hot isostatic pressing (HIP) and vacuum sintering (VS) for producing Ti-TiB was previously compared in a study examining its microstructure and properties. The sintered TiB_2 had only been mostly transformed to fine TiB whiskers in a spark plasma product. This is not unexpected given that it has been demonstrated that an electric current has an inherent effect that accelerates the diffusion and phase change dynamics [23,24]. Some recent research has investigated forging as a method of bulk deformation processing (BDP) for Ti-TiB and Ti-TiB whiskers hybrid composites [25], as well as extrusion [26,27], equally angled channels pressing [28], and hot rolling [29]. Even though there has been a lot of research on traditional constituent mixing techniques, such as casting or powder metallurgy processing, just a few studies have looked at alternative designs [23,30–32]. Numerous studies have investigated the production of Ti-TiB composites using additive laser sintering, which was discussed in a review by Attar et al. on the recent developments and opportunities in the additive manufacturing of titanium-based matrix composites [33]. Additionally, Ti-TiB_w has been discussed as a potential biomaterial and needs additional investigation [34].

However, TiB_2 is challenging to sinter to full density, hence why sintering aids are frequently needed to facilitate the liquid-phase sintering. Iron, nickel boride, and SiC have all been tested as additions, respectively [35]. Over 94% density was attained by Einarsrud et al. [36] making use of the 1700 °C pressure-free sintering. Grain size increased by 3–20 μm once Ni and NiB were introduced. The ductility of the TiB-reinforced Ti composites is a key concern. At room temperature, the composites with a TiB addition of

more than 30% show no ductility. As the amount of TiB increases, the brittleness also grows. For composites made of Ti/TiB_2, the same issue occurs. In addition to the TiB composites created from Ti powders, such as Ti alloyed with Fe-Mo, Mo, and/or Nb, high temperature modification of Ti, β phase [36], have substantially better ductility. The TiB_2 concentrations had a significant impact on the mechanical and physical characteristics [37,38]. Even at high sintering temperatures, and especially in the absence of a β stabilizer for Ti, excessive amounts of very hard TiB_2 can cause noticeable cracking in the specimens that underwent 850 °C spark plasma sintering [39]. Therefore, it is considered that using high titanium diboride concentrations without a β stabilizer is not a good idea, which is supported by a number of researchers [39–42].

Titanium Metal Composites (TMCs) can be produced using either powder metallurgy (PM) or traditional casting methods. In contrast, PM has the potential to both reduce production costs and avert casting flaws (such as coarse microstructure, shrinkage cavity, and segregation). At the same time, it allows for the near-net creation of complex-geometry components and gives users more control in how their TMCs turn out in the end [43,44].

Although Ti implants are commonly used for dental implant applications, their success depends on bone quality and quantity, the literature did not show any comparison between Ti and manufactured Ti-TiB_2 composite. Furthermore, TiB_2 has not been widely studied, with a particular focus on the dental implant applications where adequate porosity for bone osseointegration and the lightweight characteristics along with the high strength characteristics for effective mastication are required to avoid implant fracture. The main goal of the current study is to create Ti-TiB_2 composites using titanium and titanium diboride powders using the PM method for dental implant applications. This will enable the use of an implant with a small diameter in the bone to bear the strength of the occlusion and jaw muscles, which is not possible with conventional implants. Next, the composite's microstructural, physical, and mechanical characteristics including density, porosity, hardness, and compressive strength were examined.

2. Experimental

2.1. Powder Materials

Commercially pure titanium (Ti) and titanium diboride (TiB_2) powders were purchased from Hangzhou Hyper Chemicals Limited, China. Both powders are characterized by a laser particle size analyzer (Bettersize Instrument Ltd., Dandong, China), a scanning electron microscope (SEM), energy dispersive spectroscopy (EDS) (Inspect S50, FEI Company, Eindhoven, The Netherlands), and X-ray diffraction (XRD) (XRD-6000, Shimadzu, Kyoto, Japan). To provide a basic spectra of diffraction peaks, Cu K radiation at 40 kV and 40 mA was used with a scanning range between 30° and 80°.

2.2. Powder Metallurgy Procedure

2.2.1. Mold Preparation

The mold was made from stainless steel and consisted of four parts: a die, two bases, and a punch, as shown in Figure 1. The die was a hollow cylinder with a 50 mm height, a 12 mm inner diameter, and an 18 mm outer diameter. The first base was a disc with dimensions of 15 mm in height by 22 mm in diameter. At the center of the base there was a short, solid rod of 5 mm in height by 11.5 mm in diameter, which was inserted inside the hollow space of the die when it was seated on the base while pressing the powders. The second base was a hollow cylinder (35 mm height × 20 mm top inner diameter) with a 30 mm outer diameter. In a 2 mm hollow depth from the top end, there was a shoulder (3 mm width), so the inner diameter decreased to 14 mm at the beginning of the shoulder. The die putted on this shoulder after pressing to facilitate ejecting compacted samples. The punch rod used had the following dimensions: 75 mm in height and 11.5 mm in diameter. The rod is used for the compaction of powders inside the die and for ejecting the specimen outside of the die.

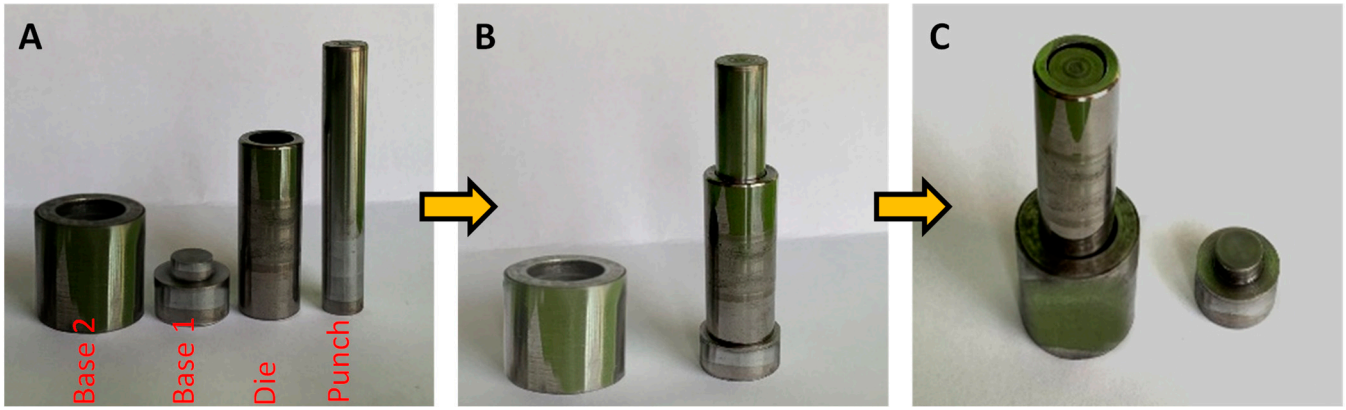

Figure 1. (**A**) parts of mold, (**B**) pressing powder position, (**C**) sample removal position.

2.2.2. Powder Preparation

The powders for groups of specimens were prepared: first, pure titanium (Ti), and second, a composite (Ti-TiB_2) of pure titanium and titanium diboride varying from 3 to 9% by weight. The mechanical mixing (pure and composite) was performed in a dry ball mill (Planetary Ball Mill, MSK-SFM-1, MTI Corporation, Richmond, CA, USA) for nearly 20 h. When mixing, stainless-steel balls outweighed the powder by a factor of 10. For further processing, the milled powder was kept in a vacuum [45].

2.2.3. Sample Preparation (Cold Compacting)

Two designs of specimens were prepared for both groups (Figure 2). The first one was for the compression test, in accordance with ASTM E9-89a (height/diameter = 1.74) [46], while the other one was for the hardness, porosity, and density characterization, in accordance with ASTM E10-15 [47] and ASTM B328-96 [48], respectively. For each test, 20 specimens were prepared: 10 for pure Ti and 10 for the composite.

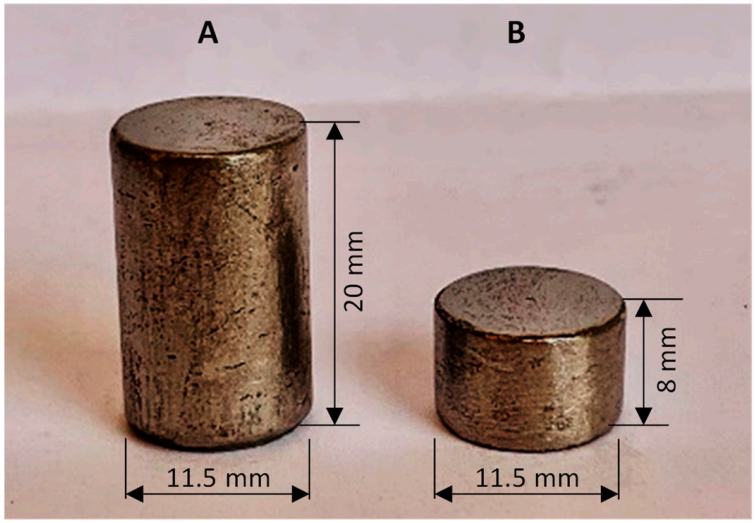

Figure 2. Study specimens: (**A**) compression, (**B**) hardness, porosity, and density.

To produce green specimens, 10 g of powder for compression (other specimens, 3.5 g) were placed in a mold to press the powder in a uniaxial manner through a hydraulic press with a digital gauge (Carver, Coeymans, NY, USA). The pressure used to determine optimum green sample density (3.151 g/cm^3) was 800 MPa, as a further increase in pressure did not show any increase in density (Figure 3).

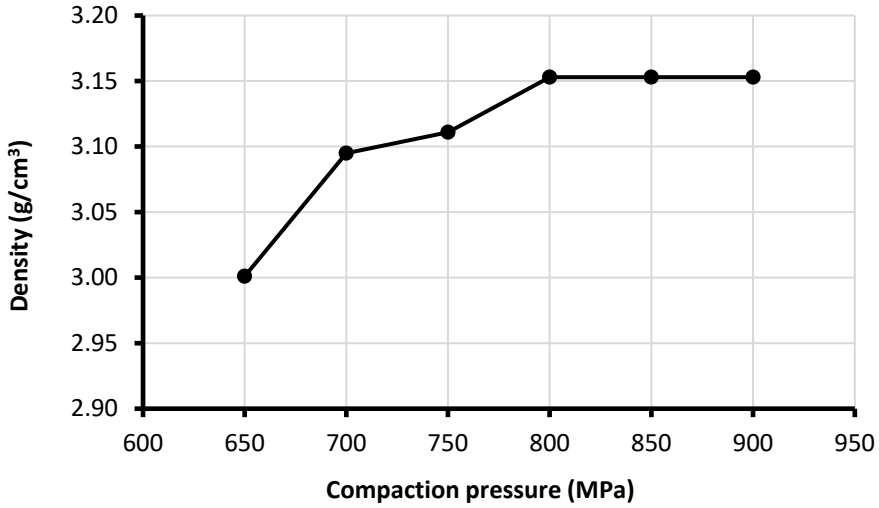

Figure 3. Variation in green sample density with compaction pressure.

2.2.4. Consolidation (Vacuum Sintering)

Sintering temperatures should be about 70% of the material's melting temperature [49]. Sintering in a vacuum tube furnace (less than or equal to 0.1 MPa) helped solidify green composite powder into cylindrical billets (Lanphan SK2, SK2-7-14TPD3, Henan, China) maintained at 1200 °C for 5 h. The TiB_2 reacted with the Ti powder and transformed into TiB during sintering [45]. Although Ti_3B_4 is typically generated at temperatures greater than 1900 °C, some have hypothesized that it represents a possible transitional step in TMCs [19,50]. The Ti_3B_4 phase is not taken into account in this study because the sintering temperature is only 1200 °C.

2.3. Sample Characterization

2.3.1. Microstructure

The microstructures of the pure and composite materials were observed using a scanning electron microscope and the elemental composition was analyzed using an energy dispersive X-ray spectroscopy (EDS) with a WD of 11.5 mm and a voltage of 25 kV. The samples were finished and polished with a special mounting holder provided with the finishing and polishing machine (no resin was used), and no surface coating was applied as the sample was made of metallic material. An XRD diffractometer was used to confirm the presence of Ti and TiB phases in the composites (Cu K radiation at 40 kV voltage, SDD detector and 40 mA current with a scanning range between 30° and 80°).

2.3.2. Compressive Strength and Hardness

The compressive strength was carried via a computer-controlled universal testing machine (WDW-200KN, Shandong, China), according to ASTM E9-89a, with a loading rate of 0.2 mm per minute. The hardness was measured via a Brinell hardness device (Wilson UH250, Brinell Hardness Tester, Braunschweig, Germany) using a load of 187.5 KP for 10 s with three indentations per sample according to ASTM E10-15 [51].

2.3.3. Porosity and Density

According to ASTM B328-96, porosity and density were calculated for the sintered samples (n = 10). The sample was weighed after 5 h of drying at 100 °C in a vacuum furnace, and this weight is shown by A. An appropriate evacuation pump was utilized to reduce the pressure and propel the oil into the sample's pores while it was entirely submerged in oil for 30 min at room temperature. B are the degraded the outcomes after weighting the

fully impregnated sample in air. The specimen that has been totally impregnated in water weighs mass is *C*. The following formulas have been used to compute porosity and density:

$$p = \left[\frac{B - A}{D_o(B - C)} \times 100\right] \times D_w \quad (1)$$

$$D = \left[\frac{B}{B - C}\right] \times D_w \quad (2)$$

where: p = porosity%, D = sample density (g/cm^3), D_o = oil density (0.9919 g/cm^3). D_w= water density at 22 °C (0.9978 g/cm^3) [52].

2.4. Statistical Analysis

The appropriate statistical procedures were utilized for analyzing and assessing the results (GraphPad Prism version 9). Descriptive statistics (box plot) and inferential statistics (unpaired *t*-test) to test the means for significance (*p*-value of less than 0.05) were generated for comparison.

3. Results and Discussion

3.1. Pilot Study Results for Determining TiB_2 wt.%

The original weight percentage of TiB_2 was determined according to a pilot study. The reported values in the literature, where increasing the concentration leads to an excessive increase in the modulus of elasticity, is not suitable in terms of the biomechanics for dental implants (stress shearing). At lower concentrations, small improvements can be made [33], but not to the extent required to solve the problems of failure or fracture of the implant, particularly at a smaller diameter. The compressive strengths of the implant materials are usually greater than their shear and tensile counterparts. The compressive strengths of the implant materials used, including polymers, metals, and ceramics, vary widely, with approximately 80 MPa for polymers, 130 MPa for metals with ductility, and 500 MPa for ceramics [53]. These materials might have a higher compressive strength than the human jawbone but are not good candidates for implants due to a higher chance of failure, particularly in the case of a small diameter or cross-sectional area, which reduces the compressive strength. Although ceramics have high compressive strength but very little ductility, a metal-ceramic composite with higher compressive strength and adequate ductility would be desirable. The pilot study results showed that the concentration of TiB_2 at 9 wt.% provided the right balance of the compressive strength, density, and porosity (Figure 4) required for dental implant applications.

3.2. Powders Characterization

Average particle sizes of the pure Ti and TiB_2 powders were found to be approximately 20 µm and 10 µm, respectively (Figure 5). SEM images reveal that the Ti powder has a larger size and more irregular shape compared with the TiB_2 powder, which is smaller and less irregular (more spherical), as shown in Figure 6. These results also support the findings from the particle size analyzer. The results of XRD and EDS show the chemical composition of both powders (Figure 7).

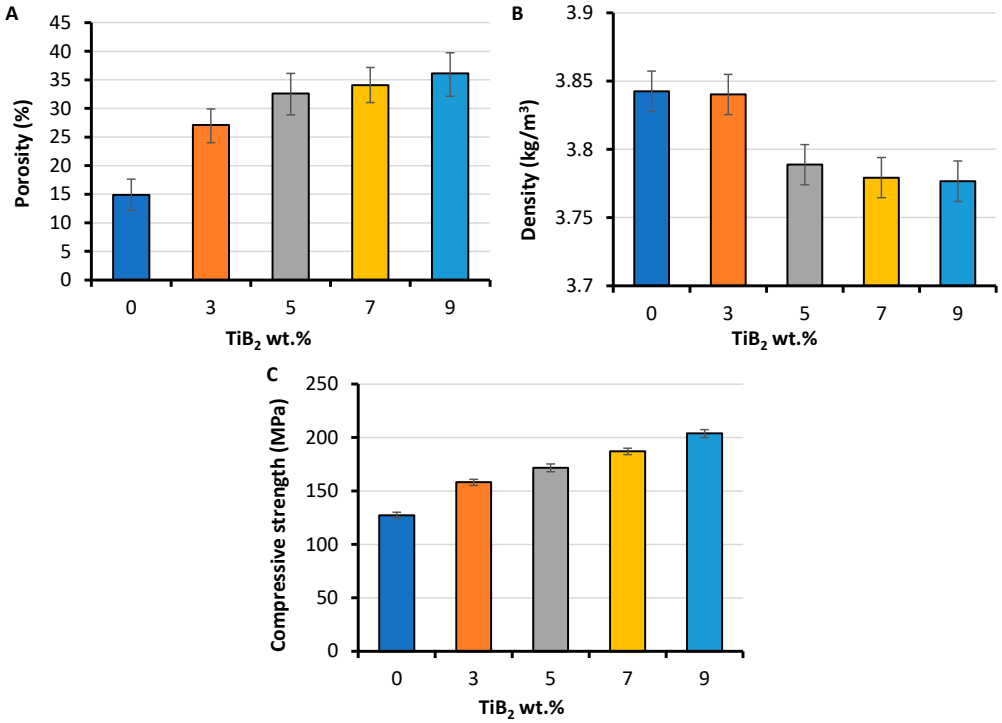

Figure 4. Pilot study on Ti-TiB_2 composites with varying wt.% of TiB_2. (**A**) porosity, (**B**) density and (**C**) compressive strength.

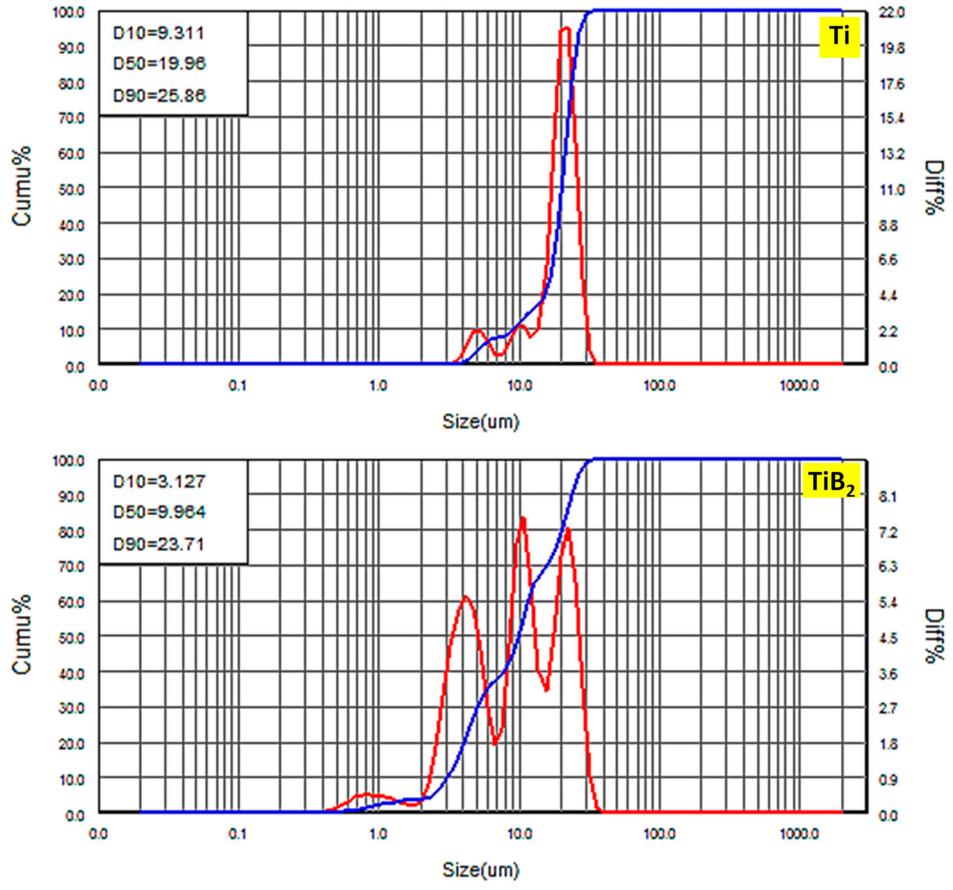

Figure 5. Particle size analysis of Ti and TiB_2 powders. The blue lines represent undersize continuous cumulative curve and the red lines represent derivative of the cumulative distribution.

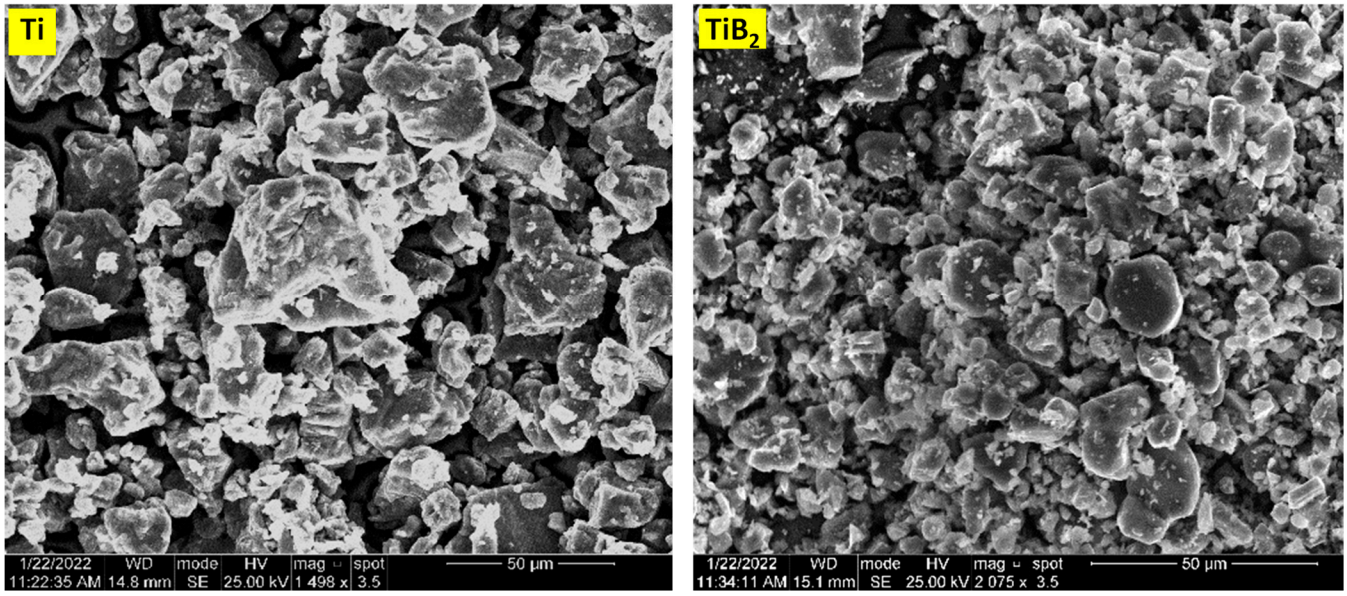

Figure 6. SEM images of Ti and TiB_2 powders.

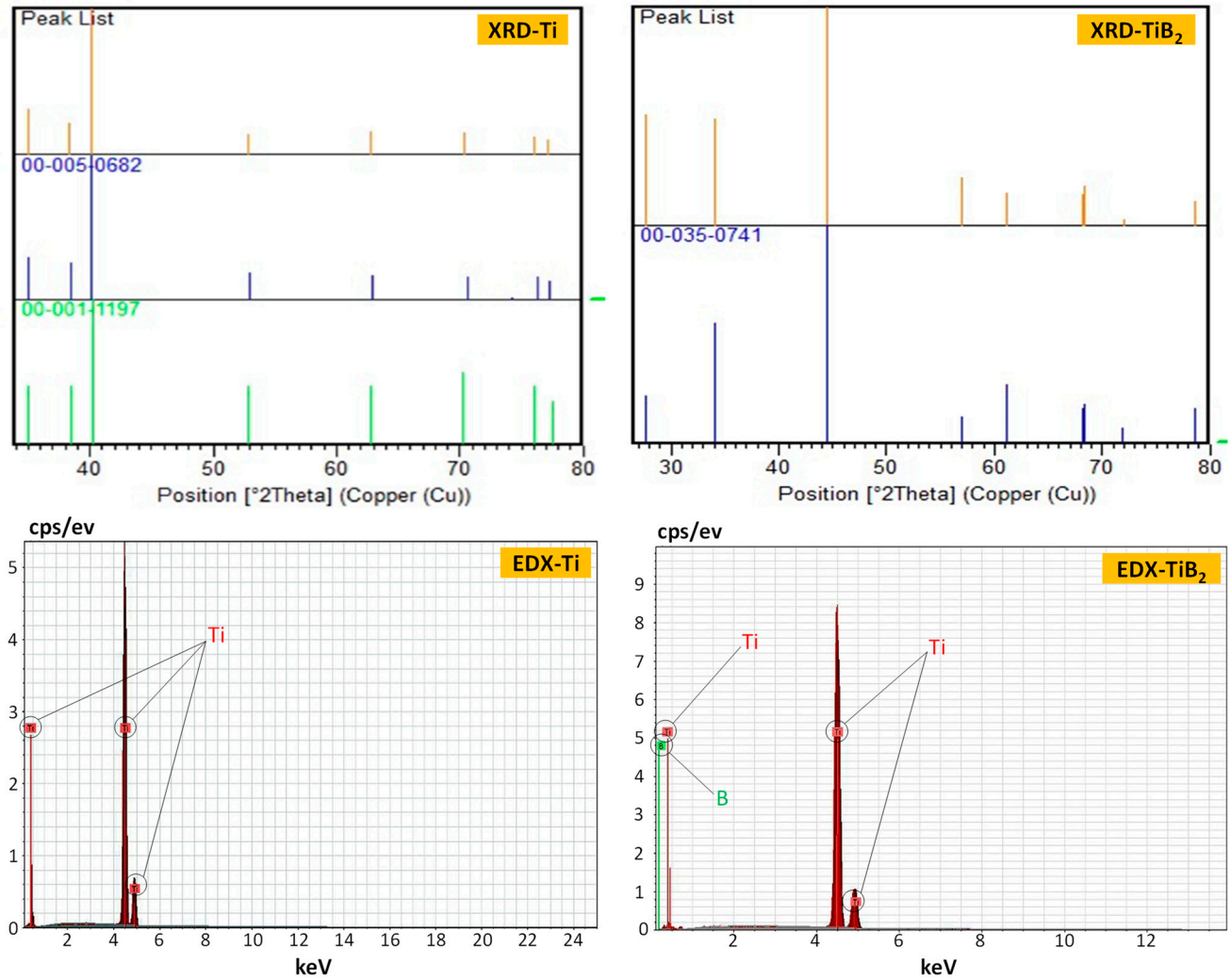

Figure 7. XRD and EDS spectra of Ti and TiB_2 powders.

3.3. Sample Microstructural Characterization

3.3.1. X-ray Diffraction Analysis

Metallographically polished samples were analyzed by XRD. Figure 8 displays the representative XRD patterns of the samples. α-Ti peaks can be seen in the composite's diffractogram confirming that the chemical process was successful. The patterns also show that the probable intermediary phase in the matrix, Ti_3B_4, does not exist [54,55]. The experiment also shows that TiB_2 particles undergo a phase transition into TiB in the matrix. Furthermore, a single TiB_2 peak (111) can be seen at 2θ = 68.326° in the XRD pattern of the composite. This finding is consistent with the slow diffusion of boron atoms in TiB reported in a previous study [45,56]. The dominant TiB (200 and 113) peaks are observed in the composites in comparison to peaks only of α Ti, in the pure sample. All composite samples have been shown to contain the same phase composition, including the hexagonally close-packed phases α-Ti and TiB. Ti (α) is the most prominent phase in all the composites. This result is consistent with that of Namini and Azadbeh [41], who observed that Ti, TiB, and TiB_2 phases were present in a Ti-TiB_2 sample. The presence of diffraction peaks of TiB in the XRD pattern confirms the in-situ reaction between Ti and TiB_2 and the formation of the TiB phase. According to studies of the Ti-TiB_2 sintering process, the presence of an excess number of titanium moles causes the thermodynamically unstable TiB_2 and Ti to react, yielding TiB [26]. Furthermore, the vacuum sintering process did not complete the chemical reaction between Ti and TiB_2 at this sintering temperature (1200 °C), as seen by the weak TiB_2 peaks that coexist with the Ti and TiB diffraction peaks. It should be noted that XRD analysis was carried out from the surface of the samples and that the results might not give the complete volumetric composition of the sample.

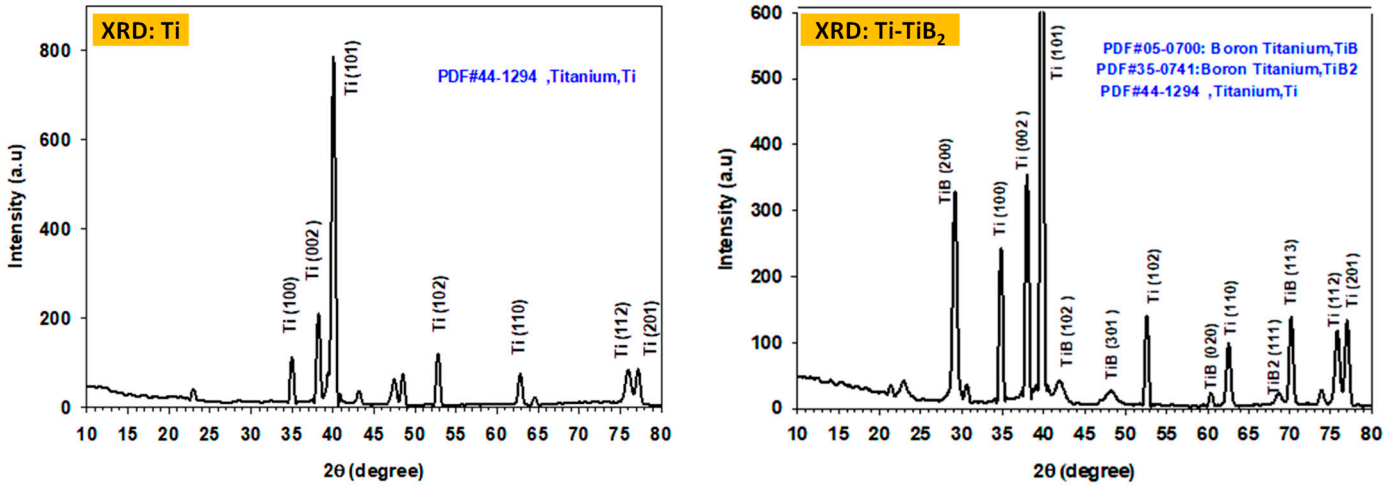

Figure 8. XRD of samples of pure Ti and Ti-TiB_2 composite.

3.3.2. Energy Dispersive Spectroscopy (EDS) Analysis

The EDS results are depicted in Figure 9 for the composite and pure samples. The results show that the composite consists of both Ti and boride phases. The figure shows two distinct regions, regardless of porosity with a color map of Ti (green) and boron (yellow) in the composite samples, in which one area is light gray indicating the presence of titanium and another is dark grey indicating the presence of boride (TiB). However, it is possible that the migration of boron atoms to the Ti-rich regions during sintering caused the appearance of a few TiB whiskers in the titanium outer matrix [45]. Pure samples only cover the light grey region (green color-map). Also, there was a very small amount of oxygen in both groups during processing indicating a low level of oxygen in the vacuum condition applied. The homogenous distribution of the B element in the analysis area indicates that the sintering process has sufficiently finished the diffusion of the element. The Ti and B enrichment in the investigated region suggests that it is in the TiB phase.

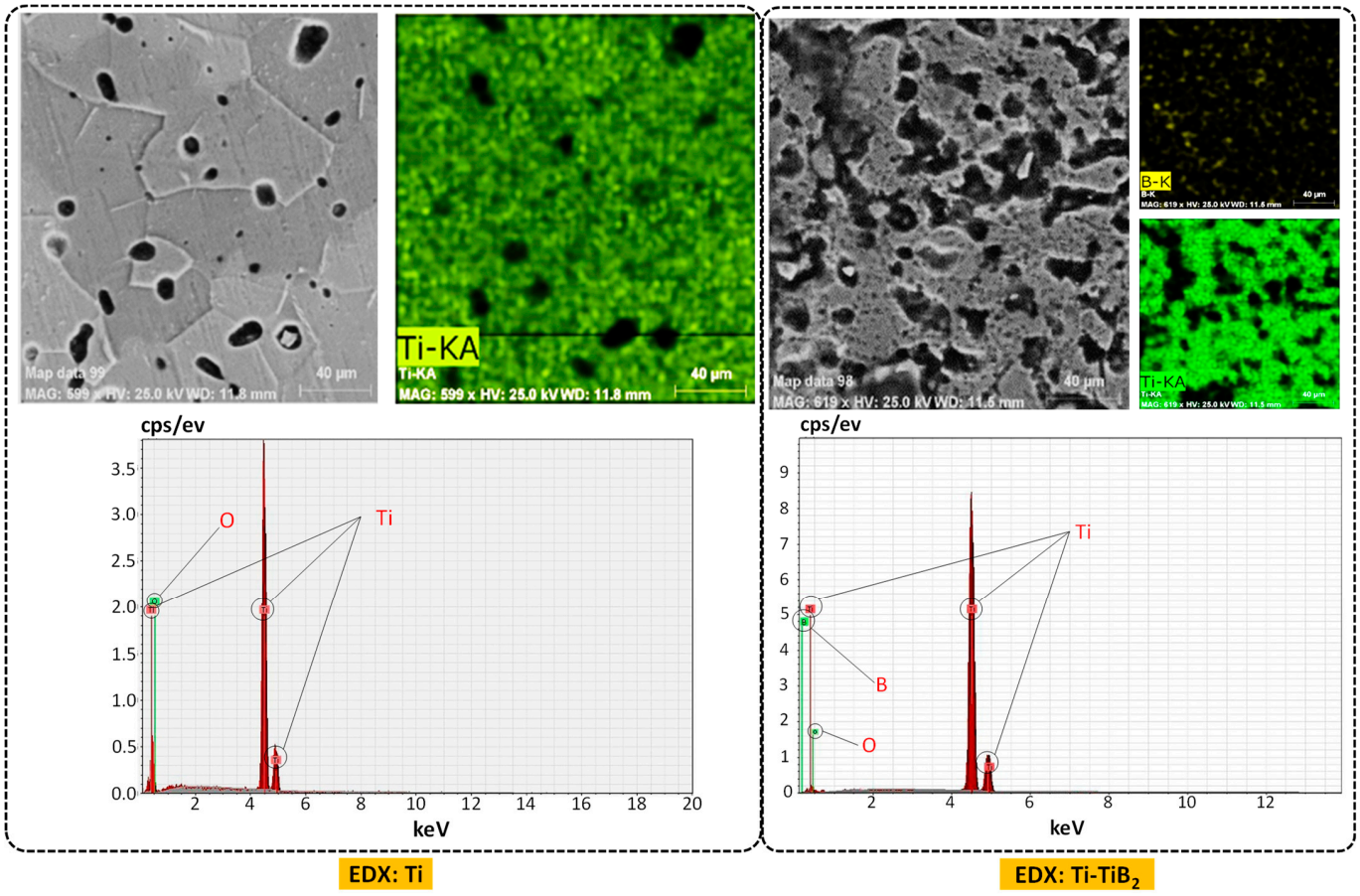

Figure 9. EDX of pure Ti and Ti-TiB_2 composite samples.

3.3.3. Scanning Electron Microscopy (SEM)

Following the sample preparation protocol, in accordance with ASTM E407-07, cross-sectional metallography and microstructures of titanium and its alloys were taken at a high-magnification using the SEM in a secondary electron detector to reveal the distribution of TiB whiskers [57,58]. Figure 10 demonstrates that the TiB whiskers are distributed throughout the composites as interconnected clusters of short whiskers, whiskers in the form of needles, and tiny plates. The composite appears to be composed of interconnected networks of short agglomerated TiB whisker clusters. Previous research has reported the presence of such groups of short TiB whiskers [45,54]. The uniform titanium is growing a few elongated TiB whiskers. In comparison, a pure sample that contains only homogeneous titanium exists without another phase of TiB.

The observation in the SEM picture of the composite reveals three colors that may be readily separated as Ti (light grey), TiB_2 (black), and TiB (dark grey). The polished surfaces of the sample are covered with random TiB whiskers. Additionally, SEM photos show unreacted TiB_2 particles clearly, which is consistent with the XRD results that were previously mentioned. The contact between the reinforcement and the matrix has a lot of pores. According to the previous study [41], the chemical reaction between Ti and TiB_2 may reduce the volume of the TiB_2 particles due to the consumption of titanium, resulting in the formation of pores.

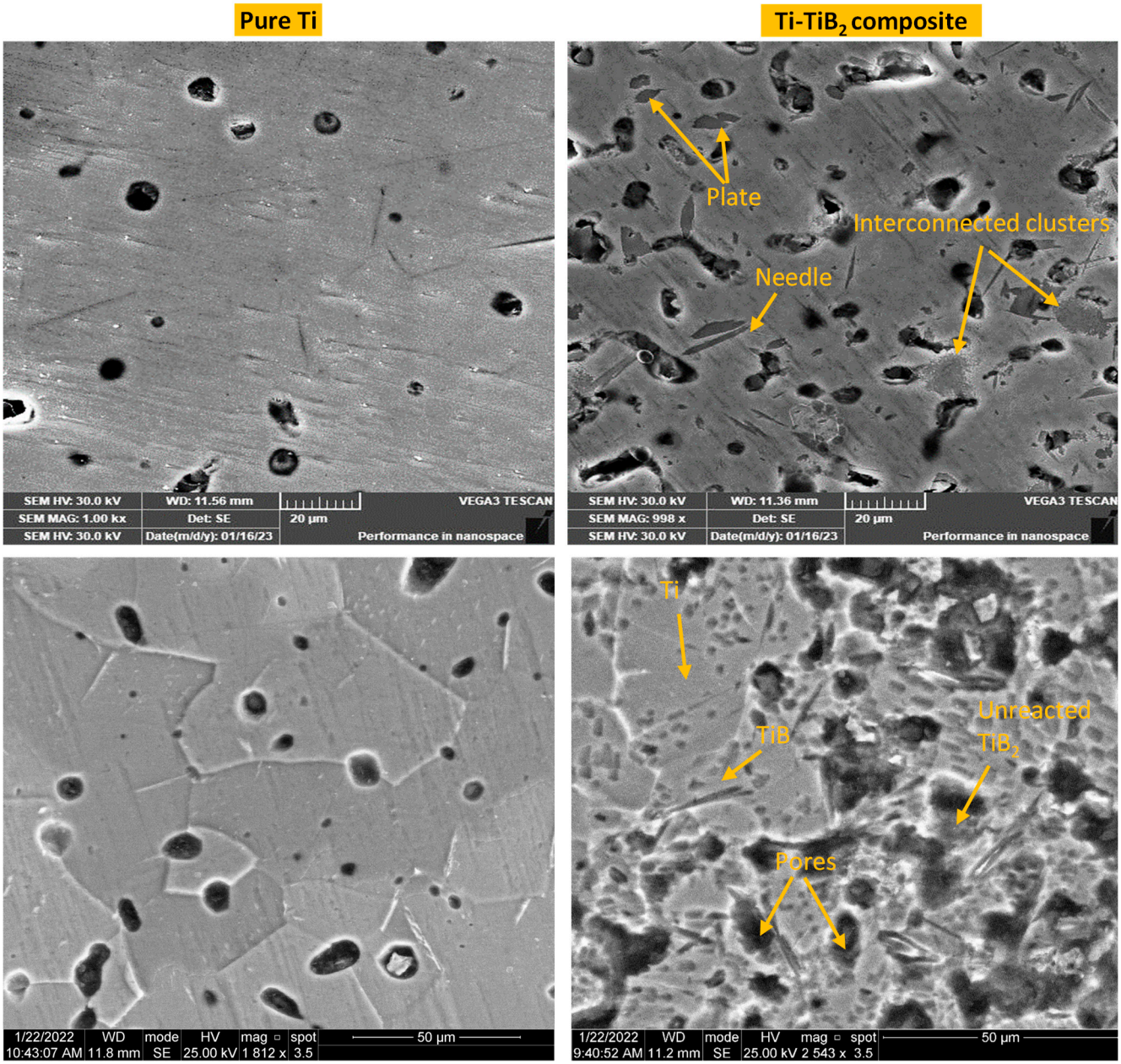

Figure 10. SEM of pure Ti and Ti-TiB_2 composite samples.

3.4. Compressive Strength and Hardness

Brinell hardness was measured for the pure and composite specimens and shown in a box plot (Figure 11a). The average hardness values (HB) of the Ti and Ti–TiB_2 composite were 221.8 ± 3.490 kg/mm^2 and 296.3 ± 2.584 kg/mm^2, respectively, which are significantly different. The increase in hardness in the composite may be explained by the function of the titanium diboride content, which forms interconnected clusters and long whiskers in the matrix, resembling needles [45,59,60]. Statistically, the star in the figure indicates a significant difference between two groups (p value < 0.0001, t = 54.25) according to an unpaired t-test.

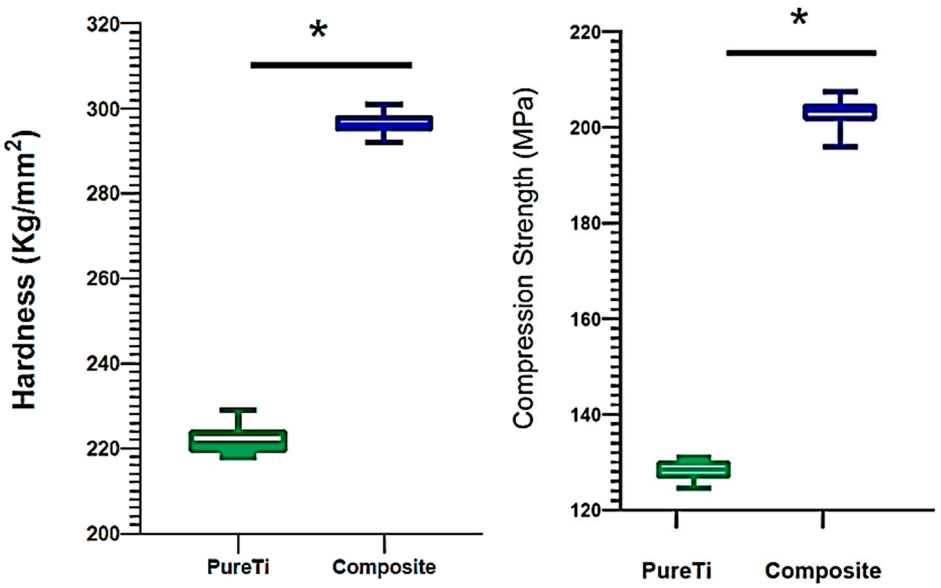

Figure 11. Box plot of (**a**) hardness and (**b**) compressive strength. The line joining two groups with a star indicates significant difference.

The mechanical characteristics are enhanced because of the in-situ production of the TiB phases. Reducing the size of the Ti grains (grain refinement) improves the room-temperature strength by creating a finer microstructure with increased hardness and strength. In general, the greater the final mechanical characteristics are, the finer the grain size [40].

Compressive strengths of the composite (203.036 ± 3.190 MPa) and pure Ti (128.293 ± 2.250 MPa) are shown in Figure 11b. It makes sense that using TiB_2 in a specific weight proportion greatly improves the compressive strength. The increased compressive strength could be linked to the following significant factors: (i) the higher filler content strength, (ii) the primary material's morphology, and (iii) the homogeneous distribution of the filler particles throughout the matrix. The superior compressive strength and the significant difference between the two groups (p value 0.0001, t = 60.55), according to an unpaired t-test, could likely be attributed to the interfacial reaction and greater consistency between the Ti matrix and filler material as a result of a higher sintering temperature, which increases atomic diffusion [61–65]. When the sintering temperature goes up, the grain size gets smaller. This makes more grain boundaries which can stop the dislocations movement and make the material stronger in compression. The increase in strength can also be attributed to five factors: (1) the solid solution atoms acting as dislocation draggers during tests, (2) the strengthening effect brought by significant grain refinement, (3) the load transfer effect of reinforcements during compressive process, (4) the mismatch of coefficient of thermal expansion (CTE) between TiB and Ti matrix, and (5) the substructure hardening resulting from increased dislocation density [15].

Grain refinement can be suspected, according to Figure 9, with the TiB content. It can be seen that some titanium is generated around the TiB phase, which might be explained by enforcing [66]. It is the non-deformable TiB particles that serve as the optimal sites for the nucleation of re-crystallized grains and the subsequent development of sub-grain boundaries as dislocations glide and gather around them during the deformation at an elevated temperature. The presence of TiB can enhance the titanium matrix's capacity for recrystallization. Furthermore, TiB particles can serve as α-Ti nucleation sites. An earlier study suggested that the orientation of TiB and α-Ti may result in the disruption of the traditional orientation relationship between titanium phases during sintering, which could

have an impact on morphology and contribute to the creation of more equiaxed grains close to TiB [67].

In general, the surface hardness and compressive strength of the titanium samples are close to the values that are reported in the literature and are relied upon as part of the properties of the titanium element, according to the discrete and stipulated test methods.

3.5. Porosity and Density

The porosity increases with an addition of the TiB_2 in the matrix, where the average porosity of the composite is 35.57% ± 0.5, and that of pure Ti is 15.50% ± 0.49 (Figure 12a). Statistically, the star indicates a significant difference between the two groups (p value < 0.0001, t = 89.18) according to the unpaired t-test. For more clarification, Figure 13 shows the SEM images that illustrate increased porosity in the composites compared to the pure Ti.

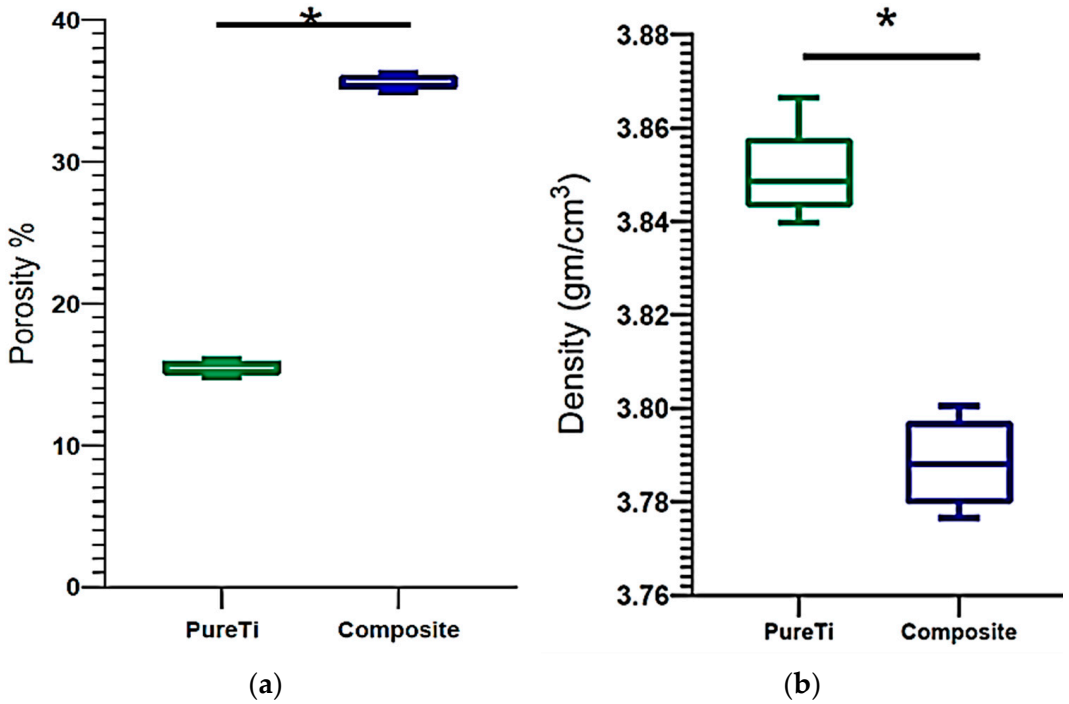

Figure 12. Box plot of (**a**) porosity and (**b**) density. The line joining two groups with a star indicates significant difference.

Conversely, density decreases with the addition of the filler content. The average density of the composite is 3.78 ± 0.0085 g/cm^3, and for the pure Ti it is 3.85 ± 0.009 g/cm^3 (Figure 12b). Statistically, the star in the figure indicates a significant difference between the two groups (p value < 0.0001, t = 15.74) according to the unpaired t-test. The plate-like TiB morphology was observed in the Ti-TiB_2 samples, and fine whiskers agglomerated with residual porosity and TiB_2. These various microstructures consequently resulted in differential porosity and density. The initial sintering temperature influenced the interface between the TiB whisker and the Ti, even though the residual TiB_2 was still present after sintering. Here, sintering in the β phase field followed by cooling through the β-α phase transformation temperature resulted in incompatible crystallo-graphic orientation relations between the matrix and the TiB whisker where there is no β-phase stabilizer of Ti, which promoted the increased local strain and dislocation density. However, these were not predicted to occur for materials sintered in the α phase field that did not have to undergo a phase change [45].

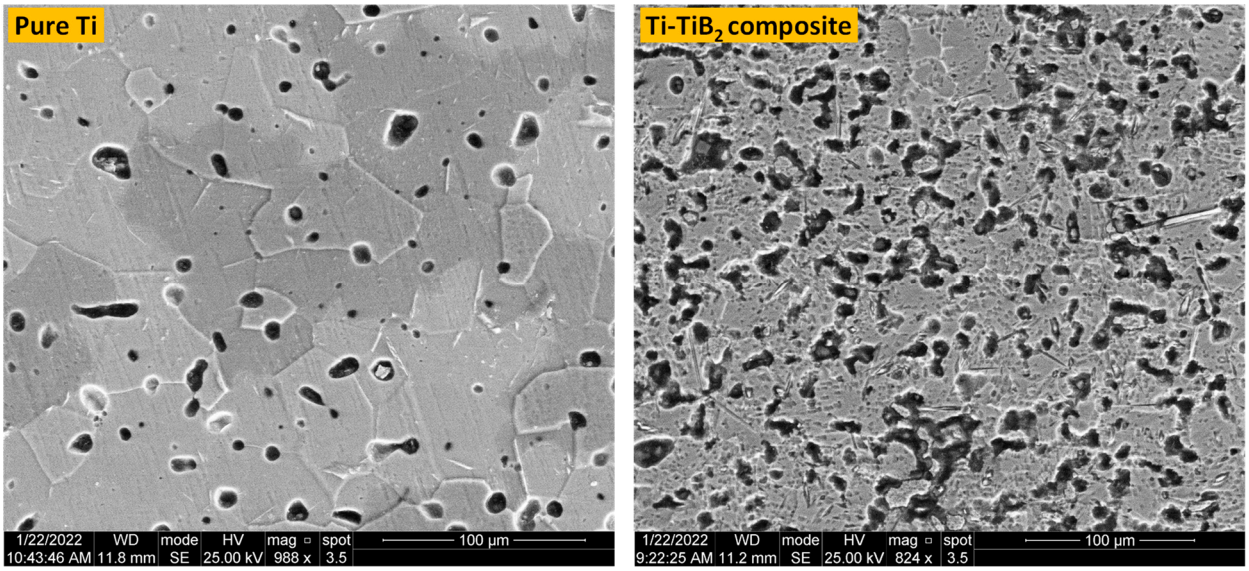

Figure 13. SEM images showing porosity in the pure Ti and composite.

Since the TiB has a lower density than both Ti and TiB_2, it was added to the formula and is likely the cause of the composite sample's lower density. Grain growth is an unavoidable side effect of conventional sintering methods, which is, in turn, attributed to the use of low heating and cooling rates in conjunction with the lengthy holding durations [19]. Sintered density falls and porosity rises (grain growth) when the sintering temperature rises further. At high sintering temperatures (1200 °C), which promote grain formation and slightly wider pores, it is clear that the porosities appear to be linked and irregularly shaped (Figure 13). Higher temperatures cause significant grain expansion and verify the decreases in the sintered density [39]. According to the reports [38,68], Ti-TiB_2 sintering results in the grain growth of α-Ti, which in turn leads to grain expansion. It should be observed that when the sintering temperature rises, beta phase (transformed at a high sintering temperature) growth outpaces alpha phase growth. By contrasting the beta (bcc) and alpha (hcp) Ti crystal lattices, we see that the beta Ti atomic packing factor is less than that of the alpha Ti. This less compacted phase facilitates diffusion, which in turn leads to grain development.

4. Conclusions

The findings of this study allow us to draw the following conclusions:

1. The Ti-TiB_2 composite and pure Ti had a predominantly α-Ti phase microstructure, both as received and after processing. TiB whiskers are developed when the Ti matrix reacts with TiB_2.
2. The pure titanium matrix can be reinforced microstructurally with TiB_2 to form Ti-TiB_2 composite with better microstructural, physical, and mechanical properties. Uniform distribution of the filler particle in the matrix was observed with the TiB phase.
3. Moreover, the addition of TiB_2 filler resulted in an increased porosity, hardness, and compressive strength, but a decreased density.
4. From the strength point of view, the developed composite could be used for dental implants due to its excellent mechanical properties, as long as it does not show any biocompatibility issues.
5. An increased porosity (light weight) would provide space for the entry of the bone cell into the implant material and would improve the connection between the bone and the material. In vivo studies are currently in process to demonstrate the suitability of the material for dental implant.

Author Contributions: Conceptualization, A.M.A.A. and A.A.F.; methodology, A.M.A.A., J.H. and A.A.F.; validation, A.A.F. and J.H.; formal analysis, A.M.A.A., A.A.F. and J.H.; investigation, A.M.A.A. and A.A.F.; data curation, A.M.A.A. and A.A.F.; writing—original draft preparation, A.M.A.A. and A.A.F.; writing—review and editing, A.M.A.A., A.A.F. and J.H.; visualization, A.M.A.A. and J.H.; supervision, A.A.F. and J.H. All authors have read and agreed to the published version of the manuscript.

Funding: This research received no external funding.

Institutional Review Board Statement: Not applicable.

Informed Consent Statement: Not applicable.

Data Availability Statement: The data presented in this study are available within the article.

Conflicts of Interest: The authors declare no conflict of interest.

References

1. Rosa, A.L.; Crippa, G.E.; De Oliveira, P.T.; Taba, M., Jr.; Lefebvre, L.P.; Beloti, M.M. Human alveolar bone cell proliferation, expression of osteoblastic phenotype, and matrix mineralization on porous titanium produced by powder metallurgy. *Clin. Oral Implant. Res.* **2009**, *20*, 472–481. [CrossRef] [PubMed]
2. Kadhim, D.R.; Hamad, T.I.; Fatalla, A.A. Use of Eggshells as Bone Grafts around Commercially Pure Titanium Implant Screws Coated with Nano Calcium Sulfate. *Int. J. Biomater.* **2022**, *2022*, 8722283. [CrossRef] [PubMed]
3. Bhattarai, S.R.; Khalil, K.A.; Dewidar, M.; Hwang, P.H.; Yi, H.K.; Kim, H.Y. Novel production method and in-vitro cell compatibility of porous Ti-6Al-4V alloy disk for hard tissue engineering. *J. Biomed. Mater. Res. Part A Off. J. Soc. Biomater. Jpn. Soc. Biomater. Aust. Soc. Biomater. Korean Soc. Biomater.* **2008**, *86*, 289–299.
4. Duraccio, D.; Mussano, F.; Faga, M.G. Biomaterials for dental implants: Current and future trends. *J. Mater. Sci.* **2015**, *50*, 4779–4812. [CrossRef]
5. Jani, G.H.; Fatalla, A.A. Characterization and Testing the properties of PEKK-Strontium-hydroxyapatite composite material. *Res. J. Pharm. Technol.* **2022**, *15*, 3034–3040. [CrossRef]
6. Jani, G.H.; Fatalla, A.A. Surface Characterization of PEKK Modified by strontium–hydroxyapatite coating as implant material Via the magnetron sputtering Deposition technique. *J. Baghdad Coll. Dent.* **2022**, *34*, 25–36. [CrossRef]
7. Mohammed, A.A.; Hamad, T.I. Assessment of Coating Zirconium Implant Material with Nanoparticles of Faujasite. *J. Baghdad Coll. Dent.* **2021**, *33*, 25–30. [CrossRef]
8. Powers, J.M.; Wataha, J.C. *Dental Materials-E-Book: Foundations and Applications*; Elsevier Health Sciences: Amsterdam, The Netherlands, 2015.
9. Geurs, N.C.; Vassilopoulos, P.J.; Reddy, M.S. Soft tissue considerations in implant site development. *Oral Maxillofac. Surg. Clin.* **2010**, *22*, 387–405. [CrossRef]
10. Grandin, H.M.; Berner, S.; Dard, M. A review of titanium zirconium (TiZr) alloys for use in endosseous dental implants. *Materials* **2012**, *5*, 1348–1360. [CrossRef]
11. Jin, J.; Zhou, S.; Zhao, Y.; Zhang, Q.; Wang, X.; Li, W.; Chen, D.; Zhang, L.-C. Refined microstructure and enhanced wear resistance of titanium matrix composites produced by selective laser melting. *Opt. Laser Technol.* **2020**, *134*, 106644. [CrossRef]
12. Ammisetti, D.K.; Kruthiventi, S.S.H. Recent trends on titanium metal matrix composites: A review. *Mater. Today Proc.* **2020**, *46*, 9730–9735. [CrossRef]
13. Asl, M.S.; Namini, A.S.; Kakroudi, M.G. Influence of silicon carbide addition on the microstructural development of hot pressed zirconium and titanium diborides. *Ceram. Int.* **2016**, *42*, 5375–5381.
14. Morsi, K.; Patel, V.V. Processing and properties of titanium–titanium boride (TiB w) matrix composites—A review. *J. Mater. Sci.* **2007**, *42*, 2037–2047. [CrossRef]
15. Zhou, Y.; Yang, F.; Chen, C.; Shao, Y.; Lu, B.; Sui, Y.; Guo, Z. Mechanical property and microstructure of in-situ TiB/Ti composites via vacuum sintering and hot rolling. *J. Alloys Compd.* **2022**, *911*, 165042. [CrossRef]
16. Xiang, T.; Ding, S.; Li, C.; Zheng, S.; Hu, W.; Wang, J.; Liu, P. Effect of current density on wettability and corrosion resistance of superhydrophobic nickel coating deposited on low carbon steel. *Mater. Des.* **2017**, *114*, 65–72. [CrossRef]
17. Thompson, S.W. Microstructural characterization of an as-quenched HSLA-100 plate steel via transmission electron microscopy. *Mater. Charact.* **2013**, *77*, 89–98. [CrossRef]
18. Ozerov, M.; Klimova, M.; Vyazmin, A.; Stepanov, N.; Zherebtsov, S. Orientation relationship in a Ti/TiB metal-matrix composite. *Mater. Lett.* **2017**, *186*, 168–170. [CrossRef]
19. Wang, T.; Gwalani, B.; Shukla, S.; Frank, M.; Mishra, R.S. Development of in situ composites via reactive friction stir processing of Ti–B4C system. *Compos. Part B Eng.* **2019**, *172*, 54–60. [CrossRef]
20. Eriksson, M.; Salamon, D.; Nygren, M.; Shen, Z. Spark plasma sintering and deformation of Ti–TiB2 composites. *Mater. Sci. Eng. A* **2008**, *475*, 101–104. [CrossRef]

21. German, R.M. *Powder Metallurgy and Particulate Materials Processing*; Metal Powder Industries Federation: Princeton, NJ, USA, 2005; p. 522. ISBN 0-9762057-1-8.
22. Selvakumar, M.; Chandrasekar, P.; Mohanraj, M.; Ravisankar, B.; Balaraju, J. Role of powder metallurgical processing and TiB reinforcement on mechanical response of Ti–TiB composites. *Mater. Lett.* **2015**, *144*, 58–61. [CrossRef]
23. Patel, V.V.; El-Desouky, A.; Garay, J.E.; Morsi, K. Pressure-less and current-activated pressure-assisted sintering of titanium dual matrix composites: Effect of reinforcement particle size. *Mater. Sci. Eng. A* **2009**, *507*, 161–166. [CrossRef]
24. Garay, J.; Anselmi-Tamburini, U.; Munir, Z. Enhanced growth of intermetallic phases in the Ni–Ti system by current effects. *Acta Mater.* **2003**, *51*, 4487–4495. [CrossRef]
25. Gaisin, R.A.; Imayev, V.M.; Imayev, R.M. Effect of hot forging on microstructure and mechanical properties of near α titanium alloy/TiB composites produced by casting. *J. Alloys Compd.* **2017**, *723*, 385–394. [CrossRef]
26. Lu, H.; Zhang, D.; Gabbitas, B.; Yang, F.; Matthews, S. Synthesis of a TiBw/Ti6Al4V composite by powder compact extrusion using a blended powder mixture. *J. Alloys Compd.* **2014**, *606*, 262–268. [CrossRef]
27. Zhang, W.; Wang, M.; Chen, W.; Feng, Y.; Yu, Y. Evolution of inhomogeneous reinforced structure in TiBw/Ti-6AL-4V composite prepared by pre-sintering and canned β extrusion. *Mater. Des.* **2015**, *88*, 471–477. [CrossRef]
28. Xiang, J.; Han, Y.; Li, J.; Qiu, P.; Sun, X.; Lu, W. Microstructure characteristics of ECAP-processed (TiB + La_2O_3)/Ti-6Al-4V composites. *J. Alloys Compd.* **2017**, *726*, 57–66. [CrossRef]
29. Guo, X.; Lu, W.; Wang, L.; Qin, J. A research on the creep properties of titanium matrix composites rolled with different deformation degrees. *Mater. Des.* **2014**, *63*, 50–55. [CrossRef]
30. Morsi, K.; Patel, V.V.; Moon, K.S.; Garay, J.E. Current-activated pressure-assisted sintering (CAPAS) and nanoindentation mapping of dual matrix composites. *J. Mater. Sci.* **2008**, *43*, 050–056. [CrossRef]
31. Morsi, K.; Patel, V.V.; Naraghi, S.; Garay, J.E. Processing of titanium–titanium boride dual matrix composites. *J. Mater. Process. Technol.* **2008**, *196*, 236–242. [CrossRef]
32. Wang, B.; Huang, L.J.; Geng, L.; Yu, Z.S. Modification of microstructure and tensile property of TiBw/near-α Ti composites by tailoring TiBw distribution and heat treatment. *J. Alloys Compd.* **2017**, *690*, 424–430. [CrossRef]
33. Attar, H.; Ehtemam-Haghighi, S.; Kent, D.; Dargusch, M.S. Recent developments and opportunities in additive manufacturing of titanium-based matrix composites: A review. *Int. J. Mach. Tools Manuf.* **2018**, *133*, 85–102. [CrossRef]
34. Morsi, K. titanium–titanium boride composites. *J. Mater. Sci.* **2019**, *54*, 6753–6771. [CrossRef]
35. Einarsrud, M.-A.; Hagen, E.; Pettersen, G.; Grande, T. Pressureless sintering of titanium diboride with nickel, nickel boride, and iron additives. *J. Am. Ceram. Soc.* **2005**, *80*, 3013–3020. [CrossRef]
36. Panda, K.B.; Chandran, K.S.R. Synthesis of ductile titanium-titanium boride (Ti-TiB) composites with a beta-titanium matrix: The nature of TiB formation and composite properties. *Met. Mater. Trans. A* **2003**, *34*, 1371–1385. [CrossRef]
37. Namini, A.S.; Azadbeh, M.; Asl, M.S. Effect of TiB2 content on the characteristics of spark plasma sintered Ti–TiBw composites. *Adv. Powder Technol.* **2017**, *28*, 1564–1572. [CrossRef]
38. Asl, M.S.; Namini, A.S.; Motallebzadeh, A.; Azadbeh, M. Effects of sintering temperature on microstructure and mechanical properties of spark plasma sintered titanium. *Mater. Chem. Phys.* **2018**, *203*, 266–273.
39. Ozerov, M.; Klimova, M.; Kolesnikov, A.; Stepanov, N.; Zherebtsov, S. Deformation behavior and microstructure evolution of a Ti/TiB metal-matrix composite during high-temperature compression tests. *Mater. Des.* **2016**, *112*, 17–26. [CrossRef]
40. Mohammadzadeh, A.; Namini, A.S.; Azadbeh, M.; Motallebzadeh, A. On the physical and mechanical properties of spark plasma sintered pure Ti and Ti-TiB composite. *Mater. Res. Express* **2018**, *5*, 126512. [CrossRef]
41. Sabahi Namini, A.; Azadbeh, M. Microstructural characterisation and mechanical properties of spark plasma-sintered TiB2-reinforced titanium matrix composite. *Powder Metall.* **2017**, *60*, 22–32. [CrossRef]
42. Ozerov, M.; Stepanov, N.; Kolesnikov, A.; Sokolovsky, V.; Zherebtsov, S. Brittle-to-ductile transition in a Ti–TiB metal-matrix composite. *Mater. Lett.* **2017**, *187*, 28–31. [CrossRef]
43. Zhang, N.; Han, X.; Sun, D.; Liu, S.; Liu, H.; Yang, W.; Wu, G. Microstructure evolution and mechanical properties of LaB6-modified Ti2AlNb alloy fabricated by blended elemental powder metallurgy. *Powder Technol.* **2020**, *369*, 334–344. [CrossRef]
44. Sergi, A.; Khan, R.H.; Irukuvarghula, S.; Meisnar, M.; Makaya, A.; Attallah, M.M. Development of Ni-base metal matrix composites by powder metallurgy hot isostatic pressing for space applications. *Adv. Powder Technol.* **2022**, *33*, 10341. [CrossRef]
45. Kumar, M.S.; Chandrasekar, P.; Chandramohan, P.; Mohanraj, M. Characterisation of titanium–titanium boride composites processed by powder metallurgy techniques. *Mater. Charact.* **2012**, *73*, 43–51. [CrossRef]
46. *ASTM I. E 9-89a*; Standard Test Methods of Compression Testing of Metallic Materials at Room Temperature. Annual Book or ASTM Standards. American Society for Testing and Materials: West Conshohocken, PA, USA, 2000.
47. *ASTM I. E10-15*; Standard Test Method for Brinell Hardness of Metallic Materials. Annual Book or ASTM Standards. American Society for Testing and Materials: West Conshohocken, PA, USA, 2015.
48. *ASTM I. B 328-96*; Standard Test Method for Density, Oil Content, and Interconnected Porosity of Sintered Metal Structural Parts and Oil-Impregnated Bearings. Annual Book or ASTM Standards. American Society for Testing and Materials: West Conshohocken, PA, USA, 2003.
49. Golla, B.R.; Bhandari, T.; Mukhopadhyay, A.; Basu, B. Titanium diboride. *Ultra-High Temp. Ceram. Mater. Extrem. Environ. Appl.* **2014**, *10*, 316–360.

50. Maseko, S.; Popoola, A.; Fayomi, O. Characterization of ceramic reinforced titanium matrix composites fabricated by spark plasma sintering for anti-ballistic applications. *Def. Technol.* **2018**, *14*, 408–411. [CrossRef]
51. Al-Murshdy, J.M.S.; Al-Deen, H.H.J.; Hussein, S.R. Investigation of the effect of indium addition on the mechanical and electrochemical properties of the Ti–15Mo biomedical alloy. *J. Bio- Tribo-Corros.* **2021**, *7*, 1–8. [CrossRef]
52. Hammood, S.A.; Al-Ethari, H.; Al-Juboori, H.A. Effect of cement kiln dust on properties of Al-base composite prepared by P/M. In Proceedings of the 2017 8th International Conference on Mechanical and Aerospace Engineering (ICMAE), Prague, Czech Republic, 22–25 July 2017; pp. 204–208.
53. Misch, C.E. *Dental Implant Prosthetics-E-Book*; Elsevier Health Sciences: Amsterdam, The Netherlands, 2004.
54. Sahay, S.S.; Ravichandran, K.S.; Atri, R.; Chen, B.; Rubin, J. Evolution of microstructure and phases in in situ processed Ti–TiB composites containing high volume fractions of TiB whiskers. *J. Mater. Res.* **1999**, *14*, 4214–4223. [CrossRef]
55. Spear, K.E.; Mcdowell, P.; Mcmahon, F. Experimental evidence for the existence of the Ti3B4 phase. *J. Am. Ceram. Soc.* **1986**, *69*, C-4. [CrossRef]
56. Kim, M.G.; Sung, S.Y.; Kim, Y. Synthesis of in-situ titanium carbide particle reinforced titanium composites. In *Materials Science Forum*; Trans Tech Publications Ltd.: Wollerau, Switzerland, 2005; Volume 475, pp. 963–966.
57. *ASTM I. E407-07*; Standard Practice for Microetching Metals and Alloys. Annual Book or ASTM Standards. American Society for Testing and Materials: West Conshohocken, PA, USA, 2011.
58. Gammon, L.M.; Briggs, R.D.; Packard, J.M.; Batson, K.W.; Boyer, R.; Domby, C.W.; ASM Handbook Committee; Aliya, D.; Lampman, S.; Stefanescu, D.M.; et al. Metallography and microstructures of titanium and its alloys. *ASM Handb.* **2004**, *9*, 899–917.
59. Gorsse, S.; Chaminade, J.; Le Petitcorps, Y. In situ preparation of titanium base composites reinforced by TiB single crystals using a powder metallurgy technique. *Compos. Part A Appl. Sci. Manuf.* **1998**, *29*, 1229–1234. [CrossRef]
60. Panda, K.B.; Ravi Chandran, K.S. Titanium-titanium boride (Ti-TiB) functionally graded materials through reaction sintering: Synthesis, microstructure, and properties. *Metall. Mater. Trans. A* **2003**, *34*, 1993–2003. [CrossRef]
61. Mohanavel, V. Mechanical and microstructural characterization of AA7178-TiB2 composites. *Mater. Test.* **2020**, *62*, 146–150. [CrossRef]
62. Vinayagam, M. Synthesis and evaluation on mechanical properties of LM4/AlN alloy based composites. *Energy Sources Part A Recovery Util. Environ. Eff.* **2022**, *44*, 1888–1897. [CrossRef]
63. Mohanavel, V.; Kumar, S.S.; Sathish, T.; Anand, K. Effect of ZrB2 content on mechanical and microstructural characterization of AA6063 aluminum matrix composites. *Mater. Today Proc.* **2018**, *5*, 13601–13605. [CrossRef]
64. Mohanavel, V.; Kumar, S.S.; Sathish, T.; Adithiyaa, T.; Mariyappan, K. Microstructure and mechanical properties of hard ceramic particulate reinforced AA7075 alloy composites via liquid metallurgy route. *Mater. Today Proc.* **2018**, *5*, 26860–26865. [CrossRef]
65. Mohanavel, V.; Rajan, K.; Arul, S.; Senthil, P.V. Production, Microstructure and Mechanical behavior of AA6351/TiB2 composite synthesized by direct melt reaction method. *Mater. Today Proc.* **2017**, *4*, 3315–3324. [CrossRef]
66. Pereloma, E.V.; Mannan, P.; Casillas, G.; Saleh, A.A. Particle stimulated nucleation during dynamic and metadynamic recrystallisation of Ni-30% Fe-Nb-C alloy. *Mater. Charact.* **2017**, *125*, 94–98. [CrossRef]
67. Nandwana, P.; Banerjee, R.; Hwang, J.Y.; Koo, M.Y.; Hong, S.H.; Tiley, J. Formation of equiaxed alpha and titanium nitride precipitates in spark plasma sintered TiB/Ti–6Al–4V composites. *Mater. Lett.* **2012**, *83*, 202–205. [CrossRef]
68. Zadra, M.; Casari, F.; Girardini, L.; Molinari, A. Microstructure and mechanical properties of cp-titanium produced by spark plasma sintering. *Powder Met.* **2008**, *51*, 59–65. [CrossRef]